NRC Research Press

NOTE

Tensile monotonic capacity of helical anchors in sand: interaction between helices

Dongxue Hao, Dong Wang, Conleth D. O'Loughlin, and Christophe Gaudin

Abstract: This note examines the interaction between the helices of a multi-helix anchor in terms of the mobilized drained capacity response in tension. Assessments are made on the basis of centrifuge tests in dense silica sand, supplemented with data from existing studies. The centrifuge tests were designed to isolate potential anchor installation effects from those due to the interactions between helices. The data show that additional helices will only contribute to anchor capacity if they are located outside the region of soil mobilized in the failure mechanism of the lower helices. In the dense sand considered in these centrifuge tests, this required helices to be separated by greater than nine diameters, and hence for the lowermost helix to be located at a depth greater than nine diameters. This separation distance is much higher than suggested in previous studies, which tended to attribute the low or nil contribution of additional helices to the soil disturbance generated during anchor installation.

Key words: helical anchor, sand, capacity, centrifuge tests, plate.

Résumé : Cette note examine l'interaction entre les hélices d'une ancre multi hélices en termes de réponse en capacité drainée mobilisée. Les évaluations sont effectuées sur la base d'essais en centrifugeuse dans du sable de silice dense, complétés par des données provenant d'études existantes. Les essais en centrifugeuse ont été conçus pour isoler les effets potentiels de l'installation d'ancrage de ceux en raison des interactions entre les hélices. Les données montrent que des hélices supplémentaires ne contribueront à la capacité d'ancrage que si elles sont situées en dehors de la région du sol mobilisée dans le mécanisme de défaillance des hélices inférieures. Dans le sable dense considéré dans ces essais de centrifugation, cela impliquait de séparer les hélices de plus de neuf diamètres et donc de placer l'hélice la plus basse à une profondeur supérieure à neuf diamètres. Cette distance de séparation est beaucoup plus grande que ne le suggéraient les études précédentes, qui tendaient à attribuer la contribution faible ou nulle d'hélices supplémentaires à la perturbation du sol générée lors de l'installation de l'ancre. [Traduit par la Rédaction]

Mots-clés : ancre hélicoïdale, sable, capacité, essais en centrifugeuse, plaque.

Introduction

Helical anchors have seen widespread use in the electrical power industry and are now being increasingly considered as tie-down anchors for structures subject to uplift loading, tiebacks for slope and wall retention and as anchors for offshore structures such as pipelines, wind turbines, and wave energy converters (Merifield 2011; Byrne and Houlsby 2015; Wang et al. 2013). A helical anchor comprises a number of steel helical plates welded to a central steel shaft as shown in Fig. 1. The anchor is installed by screwing it into the soil under an applied torque and axial force. Much of the research effort on helical anchors in sand has been through experimental studies where the anchors were in some instances simplified as circular plates. These experiments were conducted at both single gravity (Baker and Kondner 1966; Murray and Geddes 1987; Ghaly et al. 1991, 1998; Ilamparuthi et al. 2002; Liu et al. 2012) and in a centrifuge (Ovesen 1981; Dickin 1988; Tagaya et al. 1988; Tsuha et al. 2012), and the results were expressed as capacity factors or anchor efficiency factors. These studies showed that the capacity of a multiple-helix anchor is much lower than the sum of the bearing resistance on each plate (i.e., anchor efficiency < 1), as assessed by measuring the capacity of single-helix anchors with each helix located at the same depth as the helices in the multiple-helix anchor. Such observations are also reflected in design guidance for helical anchors (Lutenegger 2015), which recommends progressively lower efficiency factors for the deeper helices. However, the interaction between the individual helices in multiple-helix anchor has not been analysed very well, and the low anchor efficiency was attributed to installation effects in Clemence et al. (1994), Lutenegger (2011), and Tsuha et al. (2012).

This paper isolates potential installation effects by considering centrifuge data from monotonic tensile loading tests on pre-embedded helical anchors in dry dense silica sand. The experiments involve single-plate (to provide clarity on the relevance of the helical geometry to the anchor response), single-helix, and multiple-helix anchors buried at up to 12 times the helix or plate diameter, with helix spacing in the range of one to six times the helix diameter.

Testing program

Model anchors

The centrifuge tests were conducted at 20*g* in the 3.6 m diameter beam centrifuge at The University of Western Australia (UWA).

Received 4 April 2018. Accepted 1 November 2018.

D. Hao. School of Civil Engineering and Architecture, Northeast Electric Power University, 169 Changchun Road, Jilin City, 132012, China.
D. Wang. Shandong Provincial Key Laboratory of Marine Environment and Geological Engineering, Ocean University of China, 238 Songling Road, Qingdao, 266100, China.
C.D. O'Loughlin and C. Gaudin. Centre for Offshore Foundation Systems, The University of Western Australia, 35 Stirling Hwy, Crawley, WA 6009, Australia.
Corresponding author: Dong Wang (email: dongwang@ouc.edu.cn).

Fig. 1. Helical anchor showing uppermost three helices.

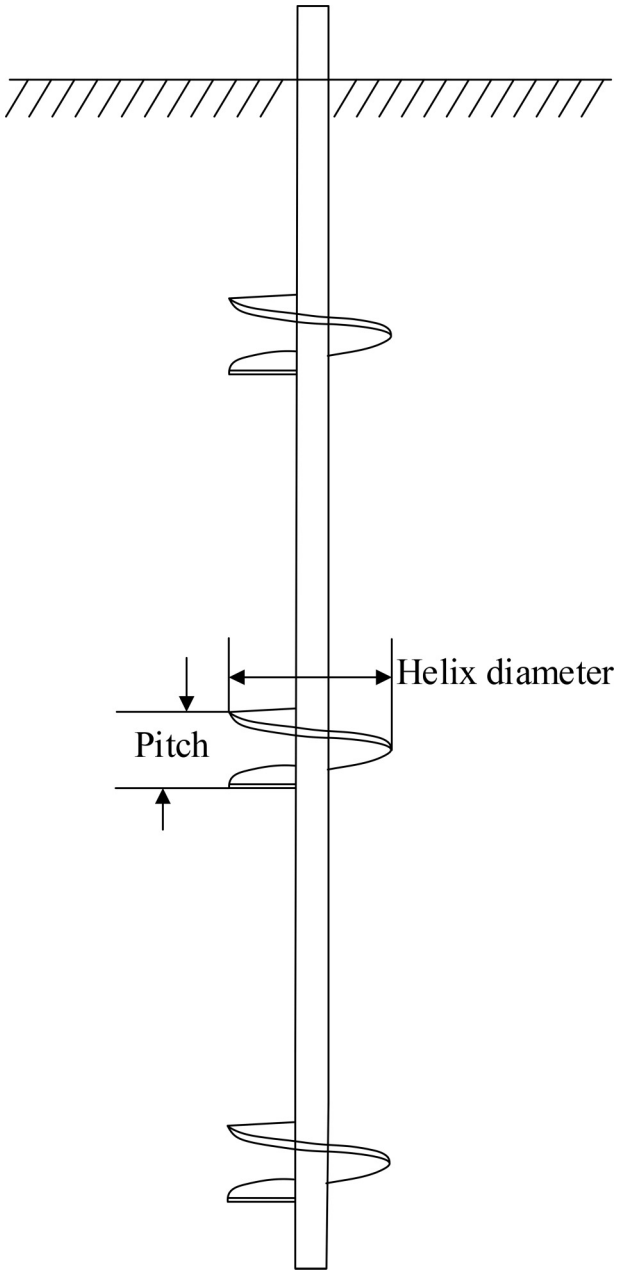

The model anchors were modular, assembled from individual helices or plates with interconnecting shafts, allowing for variations on the overall anchor length and the number of helices and their spacing (see Fig. 2). The diameter of the circular plates and helices was D = 20 mm (0.4 m in prototype scale) and the pitch of the helices was 5 mm (0.1 m in prototype scale). The circular plates were fabricated from 2 mm thick aluminium and the helices were fabricated from 1 mm thick stainless steel welded to a short shaft section 10 mm in length. The interconnecting shafts were also fabricated from stainless steel with a diameter, d = 4.7 mm, such that d/D = 0.235, which is sufficiently low for potential shaft resistance to be ignored (as shown experimentally in Tsuha et al. 2012).

Sample preparation

The soil sample was a dry fine to medium subangular silica sand with properties as listed in Table 1. The sand samples were prepared at single gravity in centrifuge sample containers measuring 650 mm × 390 mm × 325 mm (length × width × depth) by air pluviation to give final sample heights of approximately 270 mm. The samples were not saturated to optimize testing productivity, noting that saturated samples were not required as drained behaviour was the focus of the testing program.

The centrifuge tests were designed as "wished-in-place" tests, to avoid potential anchor capacity reduction effects associated with anchor installation as discussed previously. This was achieved by pausing pluviation when the soil reached the targeted height for the lowermost helix or plate. At this point the plate or helix with the first shaft extension segment was located carefully on the sample surface and pluviation recommenced until the sample height reached the targeted location for the next helix. Preparing the samples in this way — rather than locating the fully assembled helical anchor in the sample initially — reduced the potential for local soil density variations around the anchor due to "umbrella" or "shadowing" effects from the upper helices. After pluviation the soil surface was vacuum levelled, and a measurement made of the sample mass. The resulting global sample relative density was D_r = 88% ± 3% for samples 1–9 and D_r = 94% ± 2% for samples 10–13. No more than four anchor tests were conducted in each sample to limit potential interaction effects between adjacent test sites. This was based on a conservatively assumed truncated cone failure surface extending from the lowermost plate or helix at an inclination of 25° (i.e., close to the assumed dilation angle as discussed later in the paper) to the vertical (Cheuk et al. 2008).

Each centrifuge sample was spun to 20g and cone penetration tests (CPTs) were conducted to characterize the sample using a 10 mm diameter model cone penetrometer. Cone resistance profiles are provided in Fig. 3, where the variations are slight between samples and consistent with variations in the measured global density.

Testing procedure and program

The monotonic uplift tests were performed using the experimental arrangement shown in Fig. 4. An actuator with two degrees of freedom (vertical and horizontal) was controlled in-flight to locate a hook fixed at the base of an axial load cell on the vertical axis of the actuator over an "anchor cap" at the top of the helical anchor. Once in position the actuator's vertical axis was moved upwards at 0.3 mm/s until either a clearly defined peak resistance was observed or the displacement reached 1D.

The testing program encompasses 32 tests across 13 centrifuge samples, with variations on the number of helices, n; the spacing between helices, S; and the embedment depth of the lowermost helix or plate, H. The testing program (see Table 2) was designed according to the following objectives:

1. Comparison between single-plate and single-helix anchors. The first group of four single-plate anchors were tested at embedment ratios H/D = 3, 6, 9, and 12, to compare with the following tests on single-helix anchors at identical embedment ratios.
2. Investigate the embedment effect for a single-helix anchor. This second group of 16 tests compares results for a single-helix anchor at embedment ratios in the range H/D = 2–12. The tests in this group also form the base cases for comparison with the multiple-helix anchors.
3. Examine the behaviour of multiple-helix anchors. The third group of 12 tests on multiple-helix anchors (eight double-helix, three triple-helix, and a single quadruple-helix) was designed to provide insight on the interdependence of helices, examining the effect on capacity due to variations of the number of helices, the embedment ratio, and the spacing ratio.

Fig. 2. Anchor models (all dimensions in millimetres). *H*, embedment depth of the lowermost helix or plate; *S*, spacing between helices. [Colour online.]

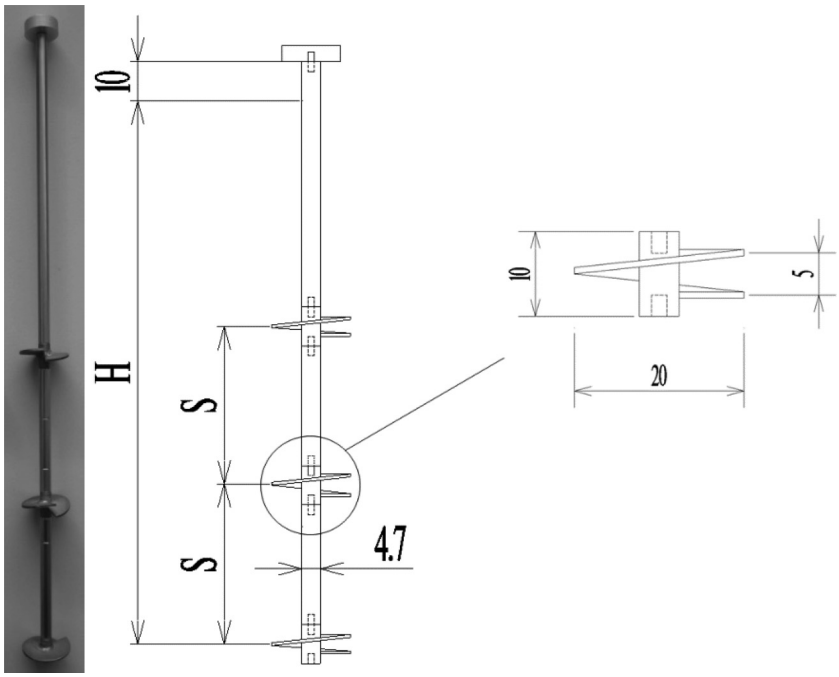

Table 1. Sand properties.

Property	Value
Specific gravity, G_s	2.65
Median grain size, d_{50} (mm)	0.25
Coefficient of uniformity, C_u	1.87
Coefficient of curvature, C_c	0.938
Maximum void ratio, e_{max}	0.703
Minimum void ratio, e_{min}	0.516
Critical state friction angle, ϕ_{cv} (°)	31

Fig. 3. Profiles of measured cone tip resistance with depth.

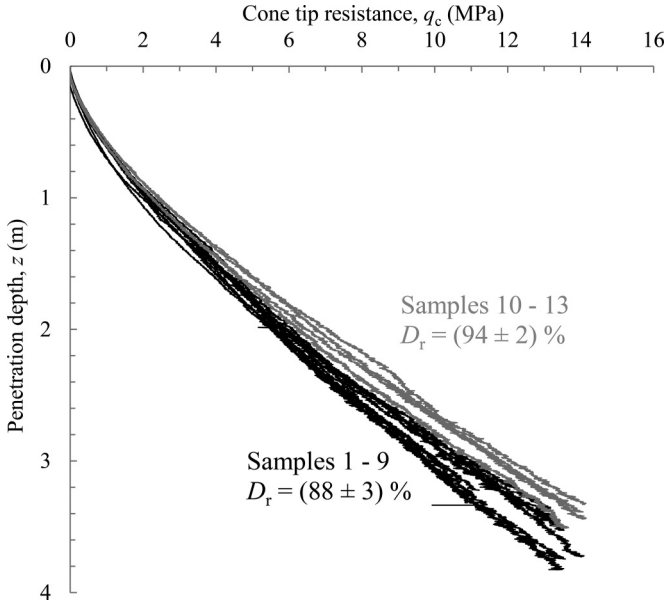

Fig. 4. Loading arrangement. [Colour online.]

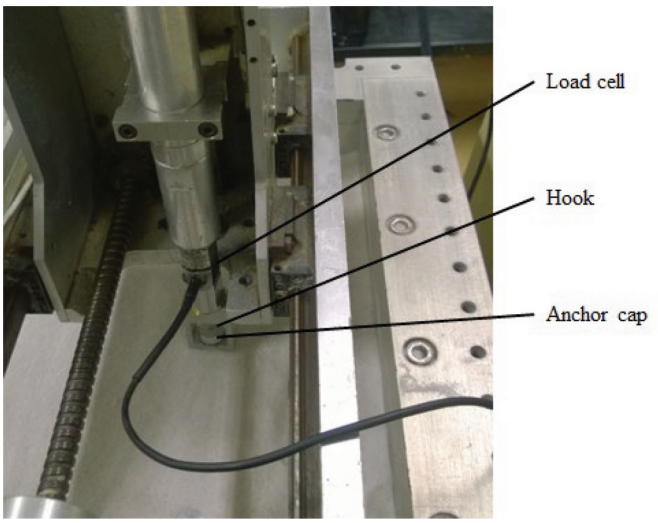

Results and discussion

The key results from the experiments are summarized in Table 2. The net ultimate anchor capacity, Q_u, was obtained by deducting the self-weight of the anchor from the peak measured uplift resistance. The anchor mobilization displacement, u_p, was taken as the anchor vertical displacement at the point where anchor capacity reached or approached a maximum, noting that post-failure load oscillations required judgement on the point of maximum anchor capacity for a number of tests. The anchor capacity factor, N_γ, was calculated as $N_\gamma = Q_u/\gamma AH$, where γ is the unit weight of sand (noting that the effective unit weight, γ', would be used for saturated conditions), A is the projected area of a single helix or plate ($A = \pi D^2/4$), and H is the embedment depth of the lowermost helix or plate as defined earlier.

Table 2. Experimental programme and key results.

Test identifier*	Plate or helix	n	S/D	H/D	Sample No.	Relative density, D_r (%)	u_p/D	Q_u (kN)	N_γ
SP3	Plate	1	—	3	2	85.8	0.050	22.9	9.0
SP6	Plate	1	—	6	2	85.8	0.140	108.7	21.3
SP9	Plate	1	—	9	2	85.8	0.204	236.2	31.0
SP12-a	Plate	1	—	12	2	85.8	0.242	357.5	35.2
SP12-b	Plate	1	—	12	6	85.4	0.238	313.4	30.8
SH2	Helix	1	—	2	9	86.7	0.032	9.9	5.8
SH3-a	Helix	1	—	3	1	86.4	0.055	22.1	8.7
SH3-b	Helix	1	—	3	13	96.2	0.067	22.9	8.9
SH4	Helix	1	—	4	9	86.7	0.091	42.9	12.6
SH6-a	Helix	1	—	6	1	86.4	0.128	108.1	21.3
SH6-b	Helix	1	—	6	13	96.2	0.146	121.7	23.6
SH7.5	Helix	1	—	7.5	5	90.0	0.180	161.6	25.3
SH8-a	Helix	1	—	8	1	86.4	0.170	176.4	26.1
SH8-b	Helix	1	—	8	12	96.4	0.188	217.6	31.7
SH9-a	Helix	1	—	9	7	88.8	0.201	249.9	32.7
SH9-b	Helix	1	—	9	11	96.1	0.192	270.3	35.1
SH9-c	Helix	1	—	9	13	96.2	0.166	260.0	33.7
SH10	Helix	1	—	10	12	96.4	0.190	309.6	36.1
SH10.5	Helix	1	—	10.5	5	90.0	0.201	271.8	30.5
SH12-a	Helix	1	—	12	6	85.4	0.227	322.1	31.7
SH12-b	Helix	1	—	12	10	91.7	0.209	364.9	35.7
DH7.5S1.5	Helix	2	1.5	7.5	4	88.7	0.153	158.8	—
DH12S1.5	Helix	2	1.5	12	8	86.6	0.224	383.1	—
DH9S3	Helix	2	3	9	3	89.3	0.198	240.7	—
DH12S3	Helix	2	3	12	9	86.7	0.201	412.0	—
DH10.5S4.5	Helix	2	4.5	10.5	3	89.3	0.198	320.9	—
DH12S4.5	Helix	2	4.5	12	8	86.6	0.220	370.7	—
DH9S6	Helix	2	6	9	13	96.2	0.190	264.7	—
DH12S6	Helix	2	6	12	4	88.7	0.214	384.2	—
TH9S1.5	Helix	3	1.5	9	3	89.3	0.168	222.9	—
TH12S3	Helix	3	3	12	7	88.8	0.211	459.5	—
TH12S1.5	Helix	3	1.5	12	11	96.1	0.209	512.6	—
QH12S2	Helix	4	2	12	5	90.0	0.254	489.4	—

*SP, SH, DH, TH, and QH indicates single-plate, single-helix, double-helix, triple-helix, and quadruple-helix anchors, respectively; subsequent number represents embedment depth ratio, H/D; and for multiple-helix anchors, an "S" is followed by number that represents spacing ratio, S/D between helices. Repeat tests are distinguished by appending test name with "-a", "-b" or "-c" as appropriate. u_p, anchor mobilization displacement; Q_u, ultimate anchor capacity; N_γ, anchor capacity factor.

Single-helix and single-plate anchors

Load–displacement responses for single-helix anchors at different embedment ratios are compared in Fig. 5 and selected load–displacement responses for single-plate and single-helix anchors are compared in Fig. 6. The comparisons in Figs. 5 and 6 are made on tests from samples with comparable relative densities, D_r = 88% ± 3%, allowing for the following observations:

1. Anchor capacity increases with helix embedment ratio, reflecting the increasing stress level and hence soil strength with depth, as also evident from the CPT profiles in Fig. 3.
2. The load–displacement response is typical of that expected for a dense sand, exhibiting a post-peak reduction in capacity as the mobilized friction angle reduces from the peak value to the critical state value. At displacements larger than the anchor mobilization distance (i.e., $u > u_p$, where u is anchor displacement) the capacity response oscillates significantly. This is commonly observed in vertical tensile loading tests of pipes and plates in sand (e.g., Trautmann et al. 1985; Dickin 1994; Cheuk et al. 2008; O'Loughlin and Barron 2012) and is attributed to the progressive infilling of the void that develops underneath the plate. Although the oscillations appear larger as the embedment depth increases, their magnitude is reasonably consistent with the magnitude of the ultimate anchor capacity measured in each test.
3. The stiffness response of the anchor before the ultimate capacity is observed is similar for each test. However, this also means that the mobilization distances (represented by the solid symbols in Figs. 5 and 6) increase as the embedment depth (and hence anchor capacity) increases.
4. Although the pitch of the helix anchor is 25% of the diameter, the difference in the anchor capacity for single-helix and single-plate helical anchors is within 6%, with no clear bias towards a particular geometry. Similarly, there is no clear distinction in the mobilization distances for either geometry. This is consistent with experimental data reported by Ghaly et al. (1991) that show no obvious effect on anchor capacity from variations in helix geometry.

Embedment effect for single-helix anchor

As evident from Figs. 5 and 6, anchor capacity for single-helix and single-plate anchors is strongly dependent on embedment depth. This is more clearly shown by Fig. 7, in which the anchor capacity factor is plotted as a function of embedment ratio, together with data from previous centrifuge tests reported by Ovesen (1981), Dickin (1988), Tagaya et al. (1988), and Tsuha et al. (2012), and field tests reported by Sakr (2009, 2011), Lutenegger (2011), and Giampa et al. (2017). Further details of these centrifuge and field tests are provided in Tables 3 and 4, respectively. The embedment ratio in Table 3 and Fig. 7 was taken as H/D for the circular plates and H/B for the square plate used in the Dickin (1988) and Ovesen (1981) experiments, where B is the plate breadth. All the centrifuge tests compared in Fig. 7 were carried

Fig. 5. Load–displacement responses for single-helix anchors at different embedment depths in samples with D_r = 88% ± 3%. u, anchor displacement. [Colour online.]

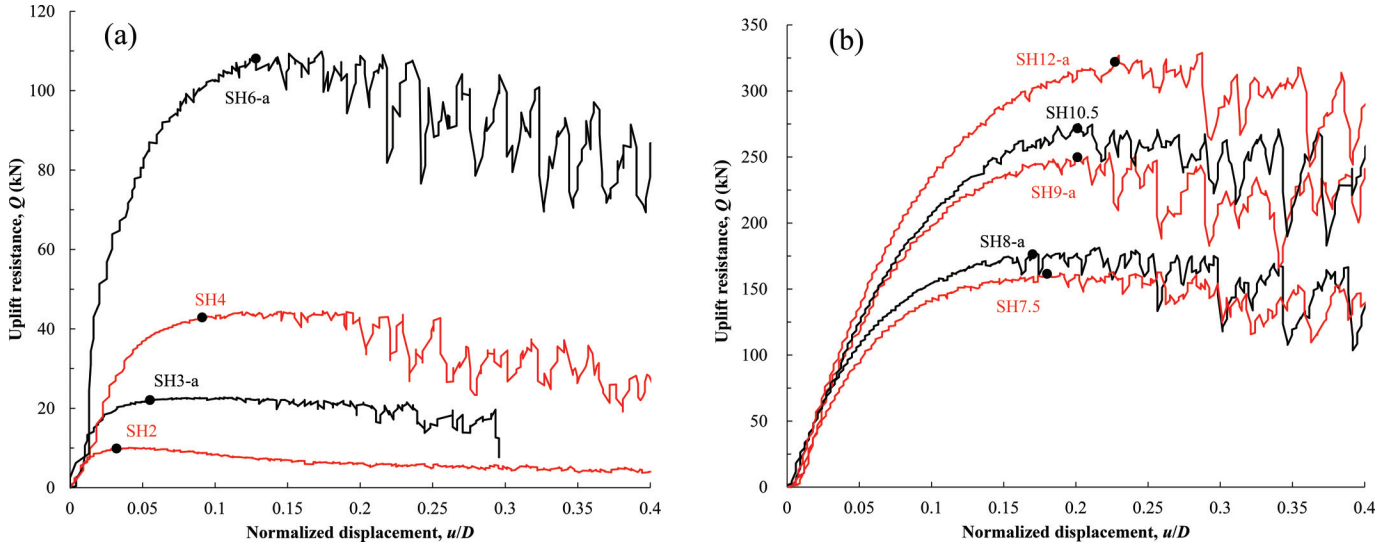

Fig. 6. Load–displacement responses for single-plate and single-helix anchors, D_r = 88% ± 3%. [Colour online.]

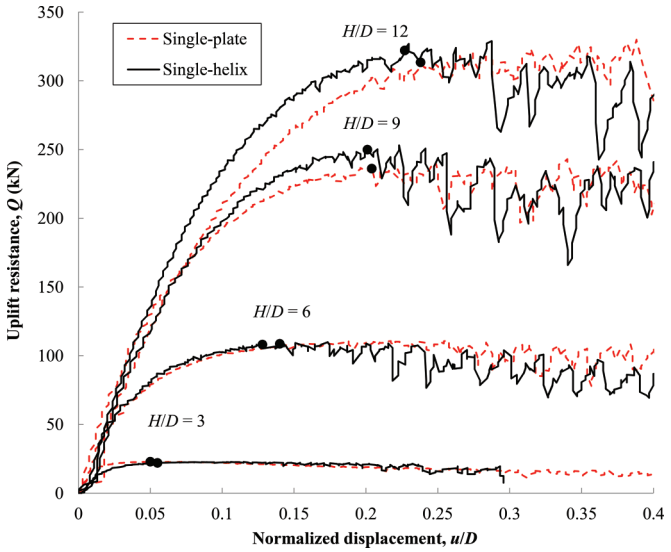

out in dense or very dense dry silica sand, with D_r > 76%. With the exception of the Giampa et al. (2017) study, the field tests were characterized by standard penetration tests, the results of which suggest dense to very dense sand in the Sakr (2009) tests, medium dense to dense sand in the Sakr (2011) tests, and medium dense sand in the Lutenegger (2011) tests. Peak friction angles were reported for each of the Giampa et al. (2017) field tests, and only tests with peak friction angles in the range ϕ_p = 45.3°–49.3° (i.e., dense to very dense) are included in Fig. 7.

The data in Fig. 7 are generally in good agreement, although the capacity factors reported in Tagaya et al. (1988) are obviously lower, which is considered to be due to the lower peak friction angle, ϕ_p, of the Ottawa sand used in the Tagaya et al. (1988) study (see Table 3), noting that a lower mobilized friction angle is also required to predict these tests, as shown later in the paper. The Sakr (2011), Lutenegger (2011), and Giampa et al. (2017) field test results are in good agreement with the centrifuge data, whilst the Sakr (2009) field test result lies above the data, which reflects the high density and strength of this sand, noting that the peak and critical state (triaxial compression) friction angles for this sand have been reported as 50° and 38°, respectively (Sharma et al. 1986).

Collectively, the data indicate that N_γ increases with embedment depth ratio, H/D, until about H/D = 9, beyond which N_γ can be considered constant (albeit with some scatter in the data, which is at least partly due to the variation in relative density). This observation supports the hypothesis that for dense sand at H/D < 9 the failure mode is shallow, with a shear failure surface that extends from the helix (or plate) to the soil surface, whereas at H/D > 9 the shear failure surfaces are likely to be constrained to a limited area above (and potentially below) the helix or plate. White et al. (2008*a*) considered H/D = 8 to be the limiting embedment depth for shallow behaviour of planar pipes, whilst noting that this threshold would change with relative density and hence dilation angle.

White et al. (2008*a*) showed good agreement between predictions and experimental measurements for a large database of uplift tests on pipes and plates, when their limit equilibrium method (LEM) was applied to a shallow inclined slip failure mechanism (see Fig. 8), with peak angles of friction and dilation selected based on Bolton's (1986, 1987) stress–dilatancy correlations. Giampa et al. (2017) extended the White et al. (2008*a*) plane strain limit equilibrium solution for axisymmetric conditions, such that it is applicable to the single-helix and single-plate anchors considered here. A variation of the Giampa et al. (2017) model is adopted here, but with the following:

- Normal stress, σ_n, on the inclined failure surfaces calculated as in the original White et al. (2008*a*) LEM, using an earth pressure coefficient given by $K_n = (1 + K_0)/2 - (1 - K_0)\cos 2\psi/2$ (where K_0 is the earth pressure coefficient at rest (= $1 - \sin\phi_{cv}$), ϕ_{cv} is the critical state friction angle, and ψ is the peak dilation angle).
- Shear stresses, τ_f, along the slip surfaces calculated using a mobilized friction angle, ϕ_m, that is lower than the peak friction angle, ϕ_p, to account for the softening induced under certain stress conditions by a nonassociated flow rule. The relationship between ϕ_m and ϕ_p is taken as $\tan\phi_m = \sin\phi_p\cos\psi/(1 - \sin\phi_p\sin\psi)$ (see Davis 1968; Drescher and Detournay 1993; Hu et al. 2014).
- Peak friction angle, ϕ_p, calculated as $\phi_p = \phi_{cv} + mI_R$, where m is the dilatancy multiplier (= 3 for triaxial conditions) and I_R is the relative dilatancy index, calculated as $I_R = 5D_r - 1$ for mean effective stress levels at failure less than 150 kPa (Bolton 1987).

Fig. 7. Anchor capacity factors for single-plate and single-helix anchors.

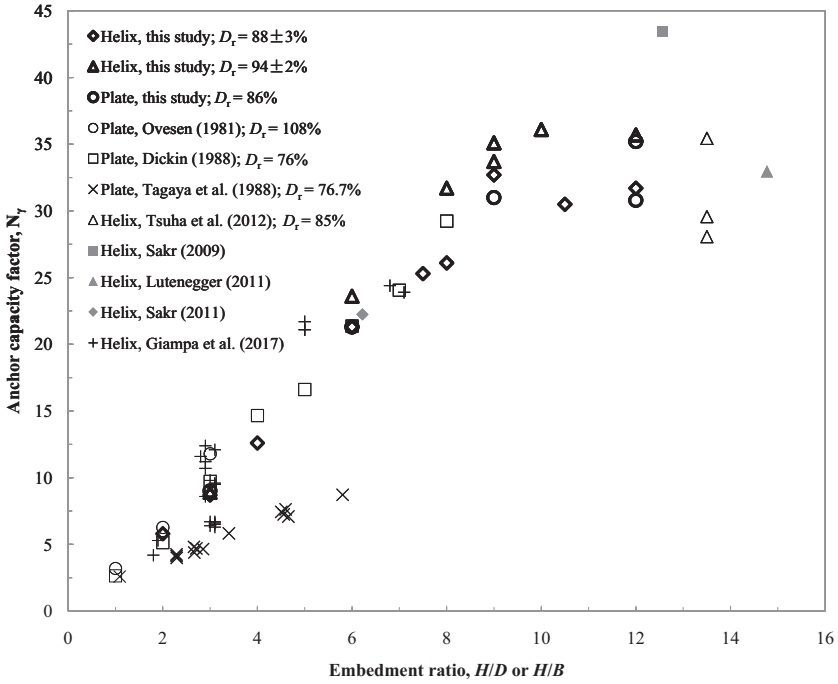

Table 3. Database of centrifuge tests.

Source	Anchor type	D or B (m)	H/D or H/B	d/D or d/B	Sand	Density, D_r (%)	ϕ_{cv} (°)	ϕ_p (°)*
Ovesen (1981)	Circular plate	1.455	1–3	—	Dansk normal sand No. 1	108†	31‡	43
Ovesen (1981)	Square plate	0.75	1.4–2.6	—	Dansk normal sand No. 1	109†	31‡	43
Dickin (1988)	Square plate	1.000	1–8	0.12	Erith sand	76	34§	46‖
Tagaya et al. (1988)	Circular plate	2.652–4.709	0.9–5.0	~0.10	Ottawa sand	76.7	29.9¶	38.4
Tsuha et al. (2012)	Circular helix	0.214–0.440	13.5	0.30	Fontainebleau sand (NE34)	85	29#	41
This study	Circular helix, circular plate	0.400	2–12	0.24	UWA sand	85–96	31**	40.8–42.4

*Estimated by Bolton's (1986) correlations.
†Reported value.
‡Assumed.
§Required m = 4.3, where m is the dilatancy multiplier, to agree with ϕ_p = 46° reported in Dickin (1988) and Dickin and King (1997).
‖As suggested in Chakraborty and Salgado (2010), triaxial ϕ_{cv} taken as 4° less than the plane strain ϕ_{cv} = 38° (Dickin 1988).
¶Reported in Negussey et al. (1988) and Guo and Su (2007).
#Reported in Gaudin et al. (2005).
**Reported in White et al. (2008*b*).

Table 4. Database of single helix anchor field tests.

Source	D (m)	H/D	d/D	Sand	Density	ϕ_{cv} (°)	ϕ_p (°)
Sakr (2009)	0.406	12.56	0.44	Alberta oil sand	Dense to very dense	38*	50*
Sakr (2011)	0.914	6.24	0.44	Northern Alberta sand	Medium dense to dense	—†	—†
Lutenegger (2011)	0.203	14.8	0.19	UMass AgFarm sand	Medium dense	—†	—†
Giampa et al. (2017)	0.152	2.9–7.1	0.23	Golden Flint sand	Dry density, γ_d = 14.7–15.8 kN/m³	33.9	45.3–49.3
	0.254	1.8–3.1	0.17	Golden Flint sand	Dry density, γ_d = 14.7–15.8 kN/m³	33.9	45.3–49.3

*Reported in Sharma et al. (1986).
†Not reported.

- The difference between the peak and critical state friction angles taken as 0.5 times the peak dilation angle, i.e., $\phi_p - \phi_{cv} = 0.5\psi$. As noted in Chakraborty and Salgado (2010), this is consistent with Bolton (1986) for triaxial conditions, and in the absence of sand-specific calibration of the stress–dilatancy relationships, is broadly appropriate for a database of different sands.

Predictions for the centrifuge data are provided in Fig. 9, and show that the LEM is an appropriate and reliable prediction method for shallowly embedded anchors. Acceptable predictions for the Dickin (1988) data required m = 4.3, giving ϕ_p = 46°, which is consistent with measured triaxial peak friction angles reported in Dickin (1988) and Dickin and King (1997), noting rather m = 3 gave a much lower ϕ_p = 42.4°. Figure 9 also shows the importance of selecting an appropriate dilation angle, ψ, as the alternate LEM predictions assuming normality ($\psi = \phi$, as required by limit theorems, e.g., Ng and Springman (1994), and is typical in finite element analyses, e.g., Merifield and Sloan (2006)) overpredict anchor capacity significantly; the LEM predictions assuming normality are higher than the LEM predictions assuming nonassociated flow by 50% at H/D = 1, increasing

Fig. 8. Inclined slip mechanism assumed in the LEM solution.

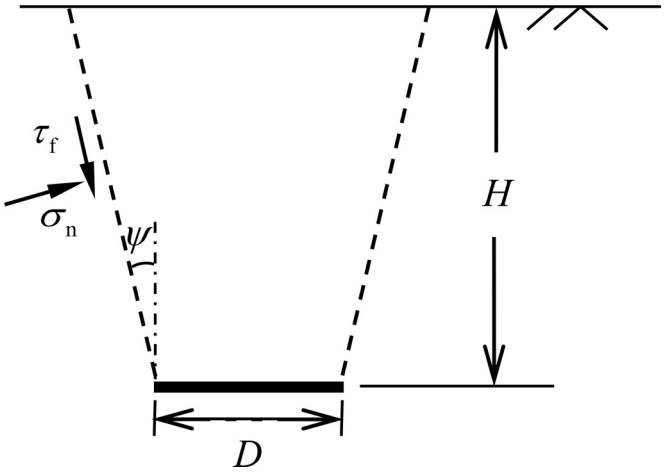

to 183% at H/D = 9. The implications of applying the LEM to deeper plate embedment are also made clear in Fig. 9*a*; for instance at H/D = 12 and for D_r = 92%, the LEM assumption of a shallow failure mechanism would lead to a calculated N_γ = 64.2 that is approximately 80% higher than the measurements.

Multiple-helix anchors

The load–displacement responses of multiple-helix anchors are compared with single-helix anchors in Fig. 10. The comparisons are made between anchors with the lowermost plate at the same embedment depth and also between samples with approximately the same relative density. Observations from Fig. 10 lead to the following comments:

1. Combinations of helices where the lowermost helix is shallower than 9*D* do not provide additional anchor capacity. This is evident from Figs. 10*a*, 10*b*, and 10*c* that compare single helix anchors with multiple helical anchors where the lowermost helix is at the same embedment depth (≤ 9*D*). In each of these comparisons the peak capacity is approximately the same. This observation indicates that when $H/D \leq 9$ the failure mechanism extends from the lowermost helix to the soil surface, such that any shallower helix is consumed within the mechanism and does not provide any additional capacity.
2. Where the lowermost helix is greater than 9*D*, additional helices provide moderate extra capacity. This is demonstrated in Fig. 10*d*, which compares a single helix anchor embedded at 10.5*D* with a double helix anchor with the lowermost plate embedded at 10.5*D* and the uppermost plate embedded at 6*D*. The difference in the peak capacity is approximately 18%, which suggests that the single helix embedded at 10.5*D* mobilizes soil above the helix to a height that does not extend to the surface (supported by Fig. 7), whereas the combination of helices at 10.5*D* and 6*D* allows soil to be mobilized to the surface. Similar conclusions can be drawn from the comparison of SH12-b and TH12S1.5 in Fig. 10*e*, where the triple helix plate provides an increase in peak capacity of 40% as the uppermost plate is at H/D = 9 and is likely to mobilize soil to the surface whereas the extent of mobilization appears to be limited in the case of the single helix anchor. A further comparison is provided in Fig. 10*f*, which compares a single helical anchor embedded at 12*D* with triple and quadruple helical anchors embedded such that the lowermost plate is also at 12*D*. The triple and quadruple helix anchors provide approximately the same capacity as the uppermost and lowermost plates are at the same embedment depth (6*D* and 12*D*, respectively). This capacity is 34% greater than that provided by the single helical anchor embedded at 12*D* as the soil mobilized by the lowermost helix does not extend to the soil surface, whereas the soil mobilized by the shallower helices does.
3. When the helix spacing is less than or equal to 2*D* the post-peak capacity softens significantly and does not exhibit the oscillations associated with progressive infilling of voids that develop beneath the helix. This is evident from Figs. 10*a*, 10*b*, 10*e*, and 10*f* and suggests that the sand is "trapped" between the helices, preventing the development of voids beneath the helices, although a void may still develop beneath the lowermost helix.
4. The pre-peak stiffness response is similar for single and multiple-helix anchors when the lowermost helix is no greater than 9*D* (see Figs. 10*a*, 10*b*, and 10*c*), but at greater embedment depths the stiffness is higher for multiple-helix anchors (see Figs. 10*d*, 10*e*, and 10*f*).

In summary, the multiple-helix anchor tests show that an additional helix will only provide extra capacity if it is located higher than the mobilized failure mechanism of the helix underneath. The separation distance for these tests in dense sand appears to be 9*D*, consistent with the transition depth between shallow and deep failure modes indicated by Fig. 7. This is made clear by Fig. 11, which shows that N_γ for a multi-helix anchor exceeds N_γ for a single-helix (or single-plate) anchor at $H/D > 9$, although the improved anchor capacity for $9 \leq H/D < 12$ are masked in Fig. 11 by variations in D_r for the various tests.

Mobilization distance

Figure 12 shows that the mobilization distance, u_p, for all anchors (represented by the solid symbols in Figs. 5, 6, and 10) increases with embedment depth. Also shown in Fig. 12 are mobilization distances from the Tsuha et al. (2012) study, interpreted from the load–displacement responses as the distance where the load practically maximizes (as adopted for the centrifuge data reported here). This differs from the mobilization distances tabulated in Tsuha et al. (2012), which were selected to coincide with the maximum anchor capacity and led to unrealistically high values for some tests. Collectively the data in Fig. 12 are well captured by the following simple linear expression proposed by Wang et al. (2012) for buried pipelines:

$$\frac{u_p}{D} = M\frac{H}{D} + N \quad (1)$$

where M and N are fitting coefficients taken as M = 0.025 (as recommended in Wang et al. 2012) and N = 0. At $H/D > 8$ the mobilization distances are lower than that given by eq. (1) suggesting a mechanism change around H/D = 8 that is consistent with the stabilization of N_γ at about H/D = 9 in Fig. 7. Interestingly there is no discernible difference in the mobilization distance for single and multiple-helix anchors at $H/D > 8$, indicating that capacity mobilization may be governed by the lowermost plate.

Concluding remarks

A series of centrifuge tests on helical anchors in dense sand were conducted to assess the drained tensile capacity contribution of a multi-helix anchor relative to a single-helix (or single-plate) anchor at the same embedment depth. The tests were motivated by previous studies that attribute low anchor efficiency in multiple-helix anchors to soil disturbance during anchor installation. Potential installation effects were isolated and removed in the tests reported here by locating the anchors in the soil samples during sample preparation.

The single-helix and single-plate tests, collectively with data from the literature, indicate that in dense sands the failure mechanism is shallow up to a plate embedment of about nine times the

Fig. 9. Calculated and measured anchor capacity factors: (*a*) this study; (*b*) existing centrifuge studies. [Colour online.]

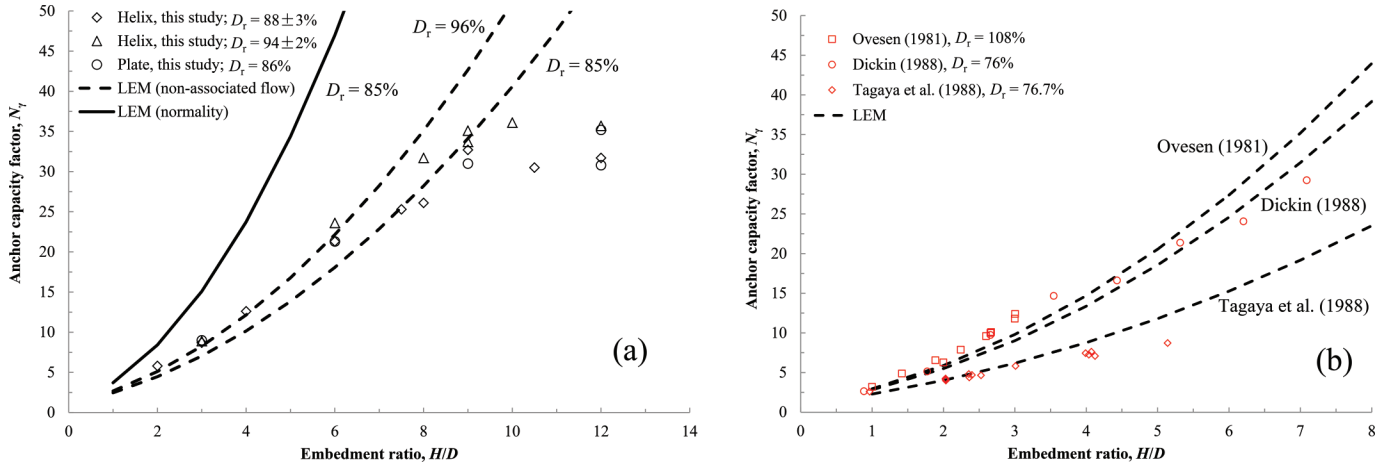

Fig. 10. Comparison between multiple- and single-helix anchors: (*a*) *H*/*D* = 7.5; (*b*) *H*/*D* = 9; (*c*) *H*/*D* = 9; (*d*) *H*/*D* = 10.5; (*e*) *H*/*D* = 12; (*f*) *H*/*D* = 12. [Colour online.]

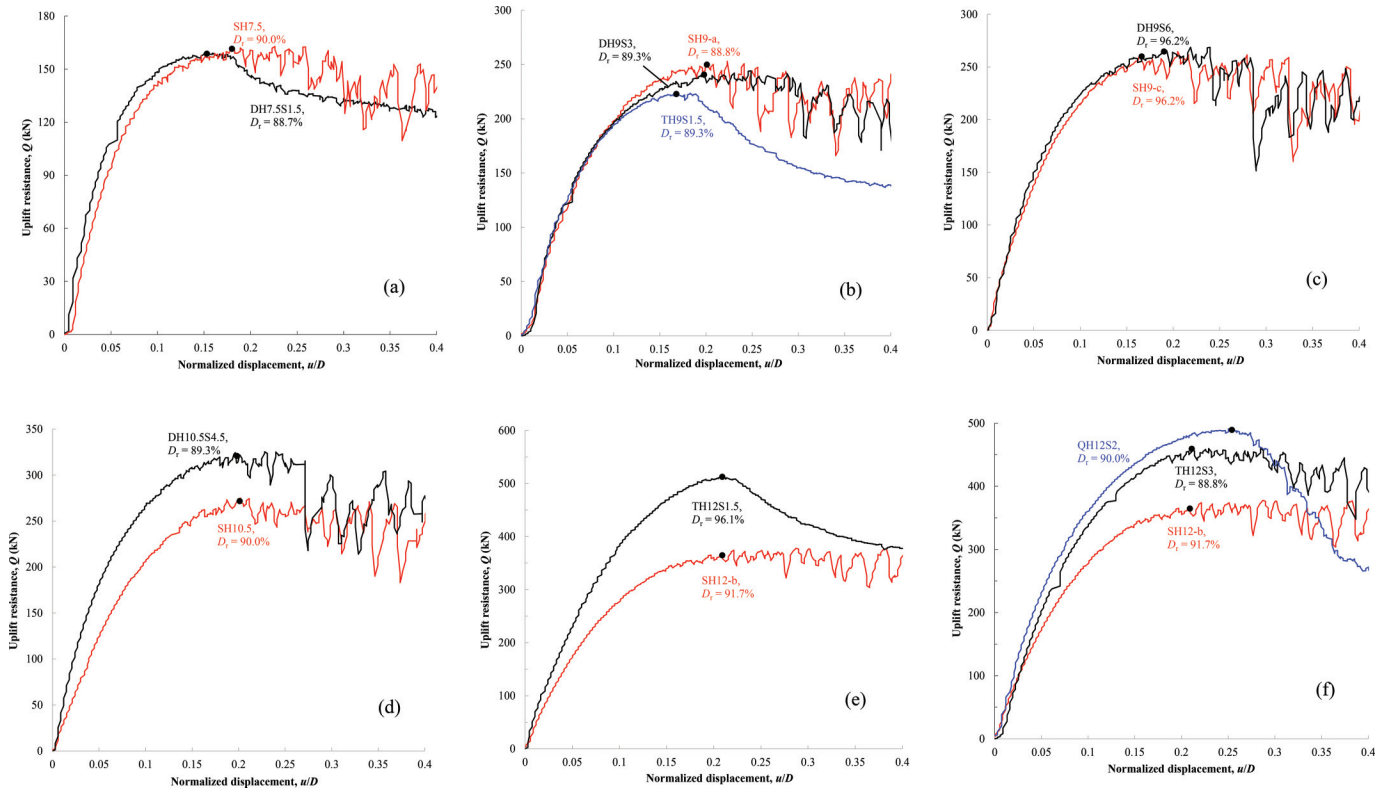

plate diameter, although it should be noted that this threshold will reduce as the relative density reduces (e.g., Tom et al. 2017).

The multiple-helix tests reveal that the contribution of additional helices relative to the lowermost helix is complex and depends on both the helix spacing and embedment depth. The most notable conclusion that can be drawn from these multiple-helix tests — which are free from installation effects — is that additional helices do not provide additional capacity if they are located within the region of soil mobilized in the failure mechanism of a lower helix. This is notable, as it confirms that the conclusion drawn in previous studies that reduced anchor efficiency is due to anchor installation effects is not the case, or at least not the sole reason for reduced anchor efficiency. It is expected that some installation effects will remain, and these may be more prevalent for deeper helices as the changes in soil state brought about during installation will be more relevant if the soil mechanism for the deeper helices is localized to the helix. The centrifuge tests show that an additional helix will only provide additional capacity when it is located at least nine diameters above the adjacent, lower helix. This spacing is entirely consistent with the transition depth between shallow and deep behaviour for a single helix (or plate), although the spacing is expected to reduce with reducing relative density.

Anchor capacity for a shallowly embedded single-plate or single-helix can be predicted reliably using a limit equilibrium approach, when peak angles of friction and dilation are selected based on Bolton's (1986, 1987) stress–dilatancy correlations. Care is required to ensure that this method is not applied beyond the

Fig. 11. Anchor capacity factors for single- and multiple-helix anchors.

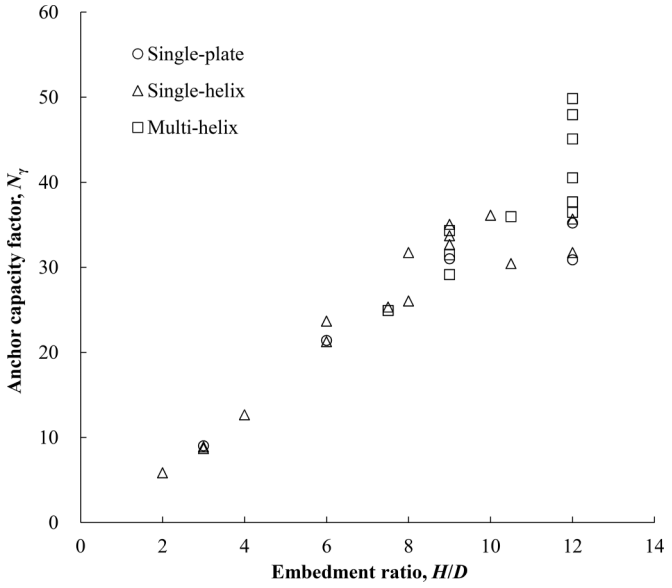

Fig. 12. Mobilization distances for single-plate, single-helix, and multiple-helix anchors. [Colour online.]

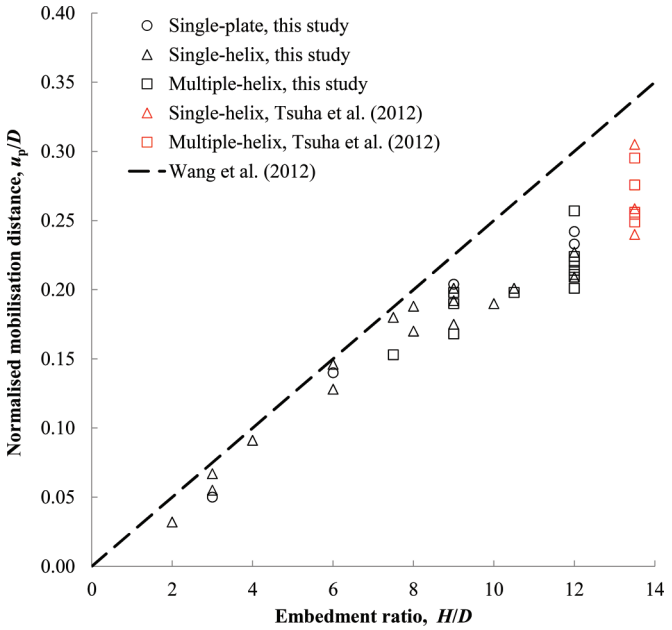

limiting embedment depth for shallow behaviour, as the resulting predictions will be unconservative. Observations from the multiple-helix anchor tests provide direction towards an appropriate prediction model for multiple-helix anchors. Experimental observations of the failure mechanism for a deeply embedded single-helix anchor and of a multiple-helix anchor would provide value in this regard.

Acknowledgements

The study formed part of the activities of the Australian Research Council Centre of Excellence for Geotechnical Science and Engineering and the Lloyd's Register Foundation (LRF) Centre of Excellence. LRF helps to protect life and property by supporting engineering-related education, public engagement, and the application of research. The first author acknowledges the financial support of National Natural Science Foundation of China (Grant No. 51308095) and the China Scholarship Council scholarship awarded for her 1 year visit to The University of Western Australia.

References

Baker, W.H., and Kondner, R.L. 1966. Pullout load capacity of a circular earth anchor buried in sand. Highway Research Record, **108**: 1–10.

Bolton, M.D. 1986. The strength and dilatancy of sands. Géotechnique, **36**(1): 65–78. doi:10.1680/geot.1986.36.1.65.

Bolton, M.D. 1987. Discussion: The strength and dilatancy of sands. Géotechnique, **37**(2): 219–226. doi:10.1680/geot.1987.37.2.219.

Byrne, B.W., and Houlsby, G.T. 2015. Helical piles: an innovative foundation design option for offshore wind turbines. Philosophical Transactions of the Royal Society A: Mathematical, Physical and Engineering Sciences, **373**(2035): 20140081. doi:10.1098/rsta.2014.0081.

Chakraborty, T., and Salgado, R. 2010. Dilatancy and shear strength of sand at low confining pressures. Journal of Geotechnical and Geoenvironmental Engineering, **136**(3): 527–532. doi:10.1061/(ASCE)GT.1943-5606.0000237.

Cheuk, C.Y., White, D.J., and Bolton, M.D. 2008. Uplift mechanisms of pipes buried in sand. Journal of Geotechnical and Geoenvironmental Engineering, **134**(2): 154–163. doi:10.1061/(ASCE)1090-0241(2008)134:2(154).

Clemence, S.P., Crouch, L.K., and Stephenson, R.W. 1994. Prediction of uplift capacity for helical anchors in sand. *In* Proceedings of the 2nd Geotechnical Conference, Cairo University, Cairo. Vol. 1, pp. 332–343.

Davis, E.H. 1968. Theories of plasticity and the failure of soil masses. *In* Soil mechanics: selected topics. *Edited by* I.K. Lee. Butterworth, London, pp. 341–380.

Dickin, E.A. 1988. Uplift behavior of horizontal anchor plates in sand. Journal of Geotechnical Engineering, **114**(11): 1300–1317. doi:10.1061/(ASCE)0733-9410(1988)114:11(1300).

Dickin, E.A. 1994. Uplift resistance of buried pipelines in sand. Soils and Foundations, **34**(2): 41–48. doi:10.3208/sandf1972.34.2_41.

Dickin, E.A., and King, G.J.W. 1997. Numerical modelling of the load-displacement behaviour of anchor walls. Computers & Structures, **63**(4): 849–858. doi:10.1016/S0045-7949(96)00066-1.

Drescher, A., and Detournay, E. 1993. Limit load in translational failure mechanisms for associative and non-associative materials. Géotechnique, **43**(3): 443–456. doi:10.1680/geot.1993.43.3.443.

Gaudin, C., Schnaid, F., and Garnier, J. 2005. Sand characterization by combined centrifuge and laboratory tests. International Journal of Physical Modelling in Geotechnics, **5**(1): 42–56. doi:10.1680/ijpmg.2005.050104.

Ghaly, A.M., and Clemence, S.P. 1998. Pullout performance of inclined helical screw anchors in sand. Journal of Geotechnical and Geoenvironmental Engineering, **124**(7): 617–627. doi:10.1061/(ASCE)1090-0241(1998)124:7(617).

Ghaly, A., Hanna, A., and Hanna, M. 1991. Uplift behavior of screw anchors in sand. I: dry sand. Journal of Geotechnical Engineering, **117**(5): 773–793. doi:10.1061/(ASCE)0733-9410(1991)117:5(773).

Giampa, J.R., Bradshaw, A.S., and Schneider, J.A. 2017. Influence of dilation angle on drained shallow circular anchor uplift capacity. International Journal of Geomechanics, **17**(2): 04016056. doi:10.1061/(ASCE)GM.1943-5622.0000725.

Guo, P., and Su, X. 2007. Shear strength, interparticle locking, and dilatancy of granular materials. Canadian Geotechnical Journal, **44**(5): 579–591. doi:10.1139/t07-010.

Hu, P., Stanier, S.A., Cassidy, M.J., and Wang, D. 2014. Predicting peak resistance of spudcan penetrating sand overlying clay. Journal of Geotechnical and Geoenvironmental Engineering, **140**(2): 04013009. doi:10.1061/(ASCE)GT.1943-5606.0001016.

Ilamparuthi, K., Dickin, E.A., and Muthukrisnaiah, K. 2002. Experimental investigation of the uplift behaviour of circular plate anchors embedded in Sand. Canadian Geotechnical Journal, **39**(3): 648–664. doi:10.1139/t02-005.

Liu, J., Liu, M., and Zhu, Z. 2012. Sand deformation around an uplift plate anchor. Journal of Geotechnical and Geoenvironmental Engineering, **138**(6): 728–737. doi:10.1061/(ASCE)GT.1943-5606.0000633.

Lutenegger, A.J. 2011. Behavior of multi-helix screw anchors in sand. *In* Proceedings of the 14th Pan-American Conference on Soil Mechanics and Geotechnical Engineering, Toronto.

Lutenegger, A.J. 2015. Quick design guide for screw piles and helical anchors in soil. International Society for Helical Foundations.

Merifield, R.S. 2011. Ultimate uplift capacity of multiplate helical type anchors in clay. Journal of Geotechnical and Geoenvironmental Engineering, **137**(7): 704–716. doi:10.1061/(ASCE)GT.1943-5606.0000478.

Merifield, R.S., and Sloan, S.W. 2006. The ultimate pullout capacity of anchors in frictional soils. Canadian Geotechnical Journal, **43**(8): 852–868. doi:10.1139/t06-052.

Murray, E.J., and Geddes, J.D. 1987. Uplift of anchor plates in sand. Journal of Geotechnical Engineering, **113**(3): 201–215. doi:10.1061/(ASCE)0733-9410(1987)113:3(202).

Negussey, D., Wijewickreme, W.K.D., and Vaid, Y.P. 1988. Constant-volume friction angle of granular materials. Canadian Geotechnical Journal, **25**(1): 50–55. doi:10.1139/t88-006.

Ng, C.W.W., and Springman, S.M. 1994. Uplift resistance of buried pipelines in granular materials. *In* Proceedings of the International Conference Centrifuge 94, Singapore, pp. 753–758.

O'Loughlin, C.D., and Barron, B. 2012. Capacity and keying response of plate anchors in sand. *In* Proceedings of the 7th International Conference on Offshore Site Investigation and geotechnics, London. SUT-OSIG-12-74.

Ovesen, N.K. 1981. Centrifuge tests of the uplift capacity of anchors. *In* Proceedings of the 10th International Conference on Soil Mechanics and Foundation Engineering, Stockholm. Vol. 1, pp. 717–722.

Sakr, M. 2009. Performance of helical piles in oil sand. Canadian Geotechnical Journal, **46**(9): 1046–1061. doi:10.1139/T09-044.

Sakr, M. 2011. Installation and performance characteristics of high capacity helical piles in cohesionless soils. DFI Journal - The Journal of the Deep Foundations Institute, **5**(1): 39–57. doi:10.1179/dfi.2011.004.

Sharma, H.D., Harris, M.C., Scott, J.D., and McAllister, K.W. 1986. Bearing capacity of bored cast-in-place concrete piles on oil sand. Journal of Geotechnical Engineering, **112**(12): 1101–1116. doi:10.1061/(ASCE)0733-9410(1986)112:12(1101).

Tagaya, K., Scott, R.F., and Aboshi, H. 1988. Pullout resistance of buried anchor in sand. Soils and Foundations, **28**(3): 114–130. doi:10.3208/sandf1972.28.3_114.

Tom, J.G., O'Loughlin, C.D., White, D.J., Haghighi, A., and Maconochie, A. 2017. Soil failure mechanisms during uplift of buried pipes, with and without radial fins. Géotechnique Letters, **7**(1): 60–67. doi:10.1680/jgele.16.00142.

Trautmann, C.H., O'Rourke, T.D., and Kulhawy, F.H. 1985. Uplift force-displacement response of buried pipe. Journal of Geotechnical Engineering, **111**(9): 1061–1076. doi:10.1061/(ASCE)0733-9410(1985)111:9(1061).

Tsuha, C.H.C., Aoki, N., Rault, G., Thorel, L., and Garnier, J. 2012. Evaluation of the efficiencies of helical anchor plates in sand by centrifuge model tests. Canadian Geotechnical Journal, **49**(9): 1102–1114. doi:10.1139/t2012-064.

Wang, D., Merifield, R.S., and Gaudin, C. 2013. Uplift behaviour of helical anchors in clay. Canadian Geotechnical Journal, **50**(6): 575–584. doi:10.1139/cgj-2012-0350.

Wang, J., Haigh, S.K., Forrest, G., and Thusyanthan, N.I. 2012. Mobilization distance for upheaval buckling of shallowly buried pipelines, Journal of Pipeline Systems Engineering and Practice, **3**(4): 106–114. doi:10.1061/(ASCE)PS.1949-1204.0000099.

White, D.J., Cheuk, C.Y., and Bolton, M.D. 2008*a*. The uplift resistance of pipes and plate anchors buried in sand. Géotechnique, **58**(10): 771–779. doi:10.1680/geot.2008.3692.

White, D.J., Teh, K.L., Leung, C.F., and Chow, Y.K. 2008*b*. A comparison of the bearing capacity of flat and conical circular foundations on sand. Géotechnique, **58**(10): 781–792. doi:10.1680/geot.2008.3781.